GLIF: A Unified Gated Leaky Integrate-and-Fire Neuron for Spiking Neural Networks

Anonymous Author(s)
Affiliation
Address
email

Abstract

Spiking Neural Networks (SNNs) have been studied over decades to incorporate their biological plausibility and leverage their promising energy efficiency. Throughout existing SNNs, the leaky integrate-and-fire (LIF) model is commonly adopted to formulate the spiking neuron and evolves into numerous variants with different biological features. However, most LIF-based neurons support only single biological feature in different neuronal behaviors, limiting their expressiveness and neuronal dynamic diversity. In this paper, we propose GLIF, a unified spiking neuron, to fuse different bio-features in different neuronal behaviors, enlarging the representation space of spiking neurons. In GLIF, gating factors, which are exploited to determine the proportion of the fused bio-features, are learnable during training. Combining all learnable membrane-related parameters, our method can make spiking neurons different and constantly changing, thus increasing the heterogeneity and adaptivity of spiking neurons. Extensive experiments on a variety of datasets demonstrate that our method obtains superior performance compared with other SNNs by simply changing their neuronal formulations to GLIF. In particular, we train a spiking ResNet-19 with GLIF and achieve 77.35% top-1 accuracy with six time steps on CIFAR-100, which has advanced the state-of-the-art.

1 Introduction

Spiking neural network (SNN) is considered the third generation of the neural network, and the bionic modeling of its activation unit is called the spiking neuron, which brings about the spike-based communication between layers[1, 2]. Due to the high sparsity and multiplication-free operation in information processing, such spike-based communication can improve energy efficiency[3, 4]. Moreover, spiking neuron can effectively capture temporal information and has good performance in processing neuromorphic data[5] and anti-noise[6]. Together with artificial neural network (ANN) colleagues, SNN further shows great potential for general intelligence[7]. Thus, SNN has aroused heated research interests recently.

The commonly used spiking neuron in different SNNs[6, 8, 9, 10, 11, 12] is the leaky integrate-and-fire (LIF) model, named vanilla LIF. As the name suggests, it can implement three different neuronal behaviors: membrane potential leakage, integration accumulation, and spike initiation. To better model neurons, prior works [13, 14, 15, 16, 17] have improved the LIF model from the above three aspects, and proposed many LIF variants with different biological features. For all the above LIF models (referred to as simplex LIF), any of the three neuronal behaviors supports only single biological feature. For instance, the vanilla LIF model only exploits exponential decay in membrane

Submitted to 36th Conference on Neural Information Processing Systems (NeurIPS 2022). Do not distribute.

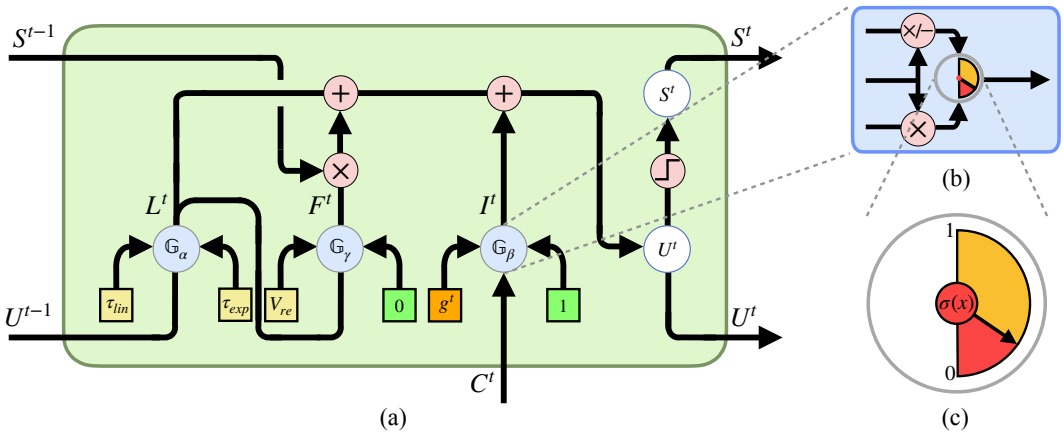

Figure 1: Illustration of the GLIF model. (a) Discrete GLIF neuron. The membrane potential U^t and the output spike S^t are updated over discrete time steps. Gating units $\mathbb{G}_\alpha$, $\mathbb{G}_\beta$, and $\mathbb{G}_\gamma$ fuse dual bio-features in membrane potential leakage, integration accumulation, and spike initiation, respectively. (b) Gating unit. (c) Gating factor.

potential leakage, while [15] only supports linear decay. However, different neurons in the cerebral cortex have different response characteristics[18, 19], especially for neurons from different brain regions. This naturally raises an issue: *could higher neuronal dynamic diversity of LIF models help SNNs do better?* In this paper, we investigate the hybrid bio-features in the LIF model to answer this question.

We propose the gated LIF model (GLIF) that fuses different bio-features in the three neuronal behaviors. As illustrated in Fig. 1, GLIF controls the fusion of different bio-features through gating units G_α, G_β, and G_γ for those three neuronal behaviors, respectively. In each gating unit, a gating factor is computed from a sigmoid function $\sigma(x)$ over a learnable gating parameter x to determine the proportion of each bio-feature, thus guiding the fusion of different bio-features. Therefore, GLIF can simultaneously contain different neuronal dynamic features, increasing the neuronal dynamic diversity of LIF models. In addition, when the gating factor is 0 or 1, GLIF can also support only single neuronal dynamic feature. As a result, GLIF can cover other different LIF models and can be viewed as a super spiking neuron, greatly enlarging the representation space of spiking neurons.

Furthermore, we introduce the channel-wise parametric method to GLIF. This method makes all membrane-related parameters in GLIF learnable and shares the same GLIF parameters channel-wisely in SNNs. Combining with learnable gating factors in GLIF, on the one hand, this method makes different channels in SNNs have completely different spiking neurons, increasing the heterogeneity of spiking neurons and the expressive ability of SNNs. On the other hand, during training, the spike neurons in SNNs are constantly changing, which is similar to the neuronal maturation during development[20, 21, 22], thus the adaptivity of spiking neurons being enhanced.

We demonstrate the effectiveness of GLIF on both static datasets and the neuromorphic dataset. Simply replacing the spiking neuron model with our GLIF in multiple networks, our model can achieve solid improvement on different tasks. For example, our model can achieve the state-of-the-art 75.48% top-1 accuracy on CIFAR-100 with only 2 time steps, which achieves the state-of-the-art results compared with other methods.

2 Related Work

Variant LIF. Variant LIF models with different biological features are proposed in previous arts, and those models differ in one or more of the three different neuronal behaviors: membrane potential leakage, integration accumulation, and spike initiation. Firstly, membrane potential leakage represents the potential decay mechanism. Exponential decay is first exploited in the vanilla LIF model[23], and

it brings neuronal dynamics with stable convergence, shrinking the potential to the resting potential steadily. But, exponential decay is not efficient enough in massive neural simulations due to its multiplication operation. Therefore, linear decay replaces exponential decay in [13, 24, 25, 26, 27], and brings neuronal dynamics with the flexibility, making it possible for configurable spiking rates [15]. Although the two decays behave differently in neuronal dynamics, both of them are proven effective in SNNs[6, 28]. Secondly, integration accumulation represents the potential accumulation induced by presynaptic spikes. Commonly, spike intensities of different time steps are considered equally high. Consequently, the discrepancies among the spikes at different time steps are ignored. To address this issue, many prior works propose to assign different weights to the input spikes at different time steps. These methods are implemented by manual settings[29, 30, 31] or adaptive settings[32, 33, 34] to improve biological plausibility, SNN performance, or inference efficiency. Lastly, spike initiation functions as the resetting mechanism triggered by spike firing. There are two common resetting strategies: hard reset[35] and soft reset[15, 36]. When a spike is triggered, the hard reset directly sets the potential to the resting potential, while the soft reset subtracts the potential by a configurable value. Therefore, hard reset is more stable as a strict reset mechanism, while soft reset is more flexible making configurable spiking rates feasible[15]. Compared with the LIF models above, our GLIF incorporates different neuronal dynamic features to increase the neuronal dynamic diversity of LIF models and improve performance of SNNs.

Parametric spiking neurons. Early existing spiking neurons often require manual tuning of the membrane-related parameters to set their neuronal dynamics, and these parameters are often shared by all neurons, which limits the diversity of spiking neurons and the expressive ability of SNNs. In recent years, Parametric spiking neurons[37, 38, 10, 28] have been proposed, which set one or more membrane-related parameters to be learnable, and update these parameters during the training of SNNs. [37] and [38] set the membrane leak and potential threshold learnable, while [10] and [28] choose the membrane leak only. FS-neuron[39] is more aggressive, setting all membrane-related parameters in the spiking neuron learnable to strictly fit the neuronal dynamics to the target activation function. Compared with the above methods, GLIF adopts the channel-wise parametric method to fully parameterize the spiking neuron, including learnable exponential decay, linear decay, potential threshold, resetting voltage, input conductance, and gating factors.

Supervised direct learning of SNNs. Supervised direct learning of SNNs follows the idea of backpropagation (BP) in ANN[40]. Bohte *et al.*[41] first adopt the surrogate gradient (SG) to empirically solve the non-differentiable term of spiking neurons by approximation with the local derivative of potential. Based on the observation that the proper steepness of the SG curve matters more than the shape in SNN learning[42], Li *et al.*[11] conduct a pre-estimation before each epoch to find the SG curve with the optimal smoothness. Besides, many techniques are developed to make deep SNNs converge faster, such as NeuNorm[8], tdBN[9], SEW block[43], TET[12], MS residual block[44], etc. In this way, the problem of end-to-end training of deep SNNs can be solved. In this paper, we choose supervised direct learning of SNNs to estimate the effectiveness of our GLIF.

3 Methodology

3.1 Revisiting LIF models

Vanilla LIF. The Vanilla LIF model is commonly adopted as a spiking neuron model in SNNs, which can be discretely formulated as follows:

$$\mathbf{U}^{(t,l)} = \tau \mathbf{U}^{(t-1,l)} \odot (1 - \mathbf{S}^{(t-1,l)}) + \mathbf{C}^{(t,l)}, \tag{1}$$

$$\mathbf{C}^{(t,l)} = \mathbf{W} \cdot \mathbf{S}^{(t,l-1)}, \tag{2}$$

$$\mathbf{S}^{(t,l)} = \mathbb{H}(\mathbf{U}^{(t,l)} - V_{th}). \tag{3}$$

Here, $\odot$ denotes the element-wise multiplication. $\mathbf{U}^{(t,l)}$ is the membrane potential vector of the layer l at time-step t and can be updated in a discrete way through Eq.(1), where $\mathbf{C}^{(t,l)}$ denotes the input vector and can be obtained by the dot-product between the synaptic weight matrix $\mathbf{W}$ and the

output spike vector of the previous layer $\mathbf{S}^{(t,l-1)}$, as described in Eq.(2). The output spike vector $\mathbf{S}^{(t,l)}$ is given by the Heaviside step function $\mathbb{H}(\cdot)$ in Eq.(3), indicating that a spike is fired when the membrane potential exceeds the potential threshold V_{th}. When updating $\mathbf{U}^{(t,l)}$ in Eq.(1), the three neuronal behaviors are considered. Specifically, the time constant τ acts as the exponential decay coefficient on the term $\tau\mathbf{U}^{(t-1,l)}$ to implement exponential decay, $\mathbf{C}^{(t,l)}$ is integrated over time to $\mathbf{U}^{(t,l)}$, and the term $(1-\mathbf{S}^{(t-1,l)})$ hard resets the membrane potential to 0 if a spike is fired at the previous time step. Notably, with all the three neuronal behaviors influencing the membrane potential, the membrane potential traces over time can explicitly depict the neuronal dynamics.

Primitives. Since each behavior is implemented by the corresponding term in formulas, for explicitness, we refer to those neural behavior related parameters as ***primitives*** in this paper. In this way, bio-features can be quantitatively described by primitives. For example, exponential decay is realized by the term $\tau\mathbf{U}^{(t-1,l)}$ in Eq.(1), so τ is a primitive and determines the amplitude of exponential decay. Thus, by choosing different primitives for each behavior, we can formulate different LIF variants. For instance, with the linear decay primitive τ_{lin} and the soft reset primitive τ_{re}, we have: $\mathbf{U}^{(t,l)} = \mathbf{U}^{(t-1,l)} - \tau_{lin} - V_{re}\mathbf{S}^{(t-1,l)} + \mathbf{C}^{(t,l)}$, which formulates the spiking neuron in [15].

3.2 Gated LIF Model

Although variant LIF offers a different choice in modeling the spiking neuron, it still remains simplex, i.e., the bio-features of the neuronal dynamic are unitary. Once formulated, a hard-reset LIF neuron cannot perform the soft-reset operation. As a result, these simplex LIF models make the spiking neurons in SNNs lack dynamic diversity. Thus, we propose the gated LIF (GLIF), a unified spiking neuron, to fuse different bio-features in the three neuronal behaviors. GLIF is illustrated in Fig. 1 and further described as follows:

$$\mathbf{U}^{(t,l)} = \mathbf{L}^{(t,l)} + \mathbf{I}^{(t,l)} + \mathbf{F}^{(t,l)} \odot \mathbf{S}^{(t-1,l)}, \tag{4}$$

$$\mathbf{C}^{(t,l)} = \mathbf{W} \cdot \mathbf{S}^{(t,l-1)}, \tag{5}$$

$$\mathbf{S}^{(t,l)} = \mathbb{H}(\mathbf{U}^{(t,l)} - V_{th}), \tag{6}$$

$$\mathbf{L}^{(t,l)} = \mathbb{G}_{\alpha}(\mathbf{U}^{(t-1,l)}; \tau_{lin}, \tau_{exp}), \tag{7}$$

$$\mathbf{I}^{(t,l)} = \mathbb{G}_{\beta}(\mathbf{C}^{(t,l)}; g^t, \mathit{1}), \tag{8}$$

$$\mathbf{F}^{(t,l)} = \mathbb{G}_{\gamma}(\mathbf{L}_{exp}^{(t,l)}; V_{re}, \mathit{0}). \tag{9}$$

In Eq.(4), $\mathbf{L}^{(t,l)}$ denotes the membrane potential vector after membrane potential leakage, $\mathbf{I}^{(t,l)}$ denotes the vector of the incremental potential caused by integration accumulation, and $\mathbf{F}^{(t,l)}$ denotes the vector of the potential reduction caused by spike initiation. Obviously, the above three vectors reflect the consequences of the three neuronal behaviors. In Eq.(7)(8)(9), the gating units $\mathbb{G}_{\alpha}(\cdot)$, $\mathbb{G}_{\beta}(\cdot)$, and $\mathbb{G}_{\gamma}(\cdot)$ are proposed to formulate the three neuronal behaviors, thus computing the consequent vectors.

Computing $\mathbf{L}^{(t,l)}$. In computing $\mathbf{L}^{(t,l)}$, the two primitives τ_{lin} and τ_{exp} are considered. τ_{lin} is the linear decay primitive, and τ_{exp} is the exponential decay primitive. As their names indicate, τ_{lin} and τ_{exp} play the roles of the linear decay and exponential decay on $\mathbf{U}^{(t-1,l)}$. Through the gating unit $\mathbb{G}_{\alpha}(\cdot)$, the two primitives are fused together to perform membrane potential leakage. Following is the formulation of $\mathbb{G}_{\alpha}(\cdot)$:

$$\mathbb{G}_{\alpha}(\mathbf{U}^{(t-1,l)}; \tau_{lin}, \tau_{exp}) = [1-\alpha(1-\tau_{exp})]\mathbf{U}^{(t-1,l)} - (1-\alpha)\tau_{lin}, \tag{10}$$

where α is the gating factor of $\mathbb{G}_{\alpha}(\cdot)$, whose value is bounded within $(0,1)$. When α approaches 0, $[1-\alpha(1-\tau_{exp})]$ and $(1-\alpha)$ tend to 1, which means GLIF performs linear decay. As α increases from 0 to 1, $(1-\alpha)\tau_{lin}$ decreases from τ_{lin} to 0, while $[1-\alpha(1-\tau_{exp})]$ decreases from 1 to τ_{exp}, which means GLIF is shifting from linear decay to exponential decay. Therefore, in Eq.(10), the two primitives τ_{lin} and τ_{exp} are dually fused with the help of the gating factor α, which can also balance the amplitudes of linear decay and exponential decay. Note that the primitives in the same gating unit

are referred to as the ***dual primitives*** in the following content, and correspondingly, the bio-features the dual primitives describe are referred to as the ***dual bio-features***. In the extreme case of $\alpha = 0$ or 1, $\mathbb{G}_\alpha$ preserves only single primitive, which means GLIF covers the simplex formulations of membrane potential leakage.

Computing $\mathbf{I}^{(t,l)}$. In computing $\mathbf{I}^{(t,l)}$, the dual primitives g^t and $\mathit{1}$ are considered to perform integration accumulation. g^t denotes the conductance primitive, namely, the time-dependent synaptic weight, which can be coded with different patterns, such as rank-order based patterns[29] and phase-coding based patterns[31]. So, we can view it as the flexible-coding primitive. While, the constant $\mathit{1}$ means $g^t \equiv 1$, representing the uniform-coding primitive, which is the dominant paradigm and proven doing well in the direct learning of SNNs[45, 12, 11]. Following is the formulation of $\mathbb{G}_\beta(\cdot)$:

$$\mathbb{G}_\beta(\mathbf{C}^{(t,l)}; g^t, \mathit{1}) = [\mathit{1} - \beta(1 - g^t)]\mathbf{C}^{(t,l)}, \tag{11}$$

where β, bounded within $(0, 1)$, is the gating factor of $\mathbb{G}_\beta(\cdot)$. Similarly, as $\beta \to 0$, the uniform-coding pattern is preferred rather than the flexible-coding, while $\beta \to 1$ is the opposite case. When $\beta = 0$ or $\beta = 1$, GLIF supports single spike coding pattern of integration accumulation.

Computing $\mathbf{F}^{(t,l)}$. In computing $\mathbf{F}^{(t,l)}$, the soft-reset primitive V_{re} and the hard-reset primitive $\mathit{0}$ are coupled as the dual primitives to perform spike initiation. Following is the formulation of $\mathbb{G}_\gamma(\cdot)$:

$$\mathbb{G}_\gamma(\mathbf{L}_{exp}^{(t,l)}; V_{re}, \mathit{0}) = -(\mathit{0} + \gamma)\mathbf{L}_{exp}^{(t,l)} - (1 - \gamma)V_{re}, \tag{12}$$

where γ bounded within $(0, 1)$ is the gating factor of $\mathbb{G}_\gamma(\cdot)$. The term $(1 - \gamma)V_{re}$ is the actual potential decrease caused by soft reset, while the term $(\mathit{0} + \gamma)\mathbf{L}_{exp}^{(t,l)}$ is the actual potential decrease caused by hard reset. Note that $\mathbf{L}_{exp}^{(t,l)}$ is given by $[1 - \alpha(1 - \tau_{exp})]\mathbf{U}^{(t-1,l)}$ in Eq.(10), which means GLIF only performs hard reset on the exponential-decay-related part of the membrane potential. In a similar way, as $\gamma \to 0$, soft reset is incrementally biased, while $\gamma \to 1$, hard reset is incrementally biased. When $\gamma = 0$ or 1, GLIF supports the simplex reset formulation of spike initiation.

Therefore, with gating units, the GLIF-based spiking neurons can fuse the dual bio-features in each one of the three neuronal behaviors. When gating factors are binary, GLIF transforms into the corresponding simplex LIFs. For example, in the case of $\alpha, \beta, \gamma = 1, 0, 1$, GLIF is equivalent to the vanilla LIF. In a nutshell, GLIF unifies different simplex LIFs by incorporating dual bio-features and exploits gating factors to balance the dual bio-features.

Channel-wise parametric method. Parametric method is applied to the primitives and gating factors in our GLIF, including τ_{lin}, τ_{exp}, V_{re}, g^t, V_{th}, α, β, and γ. We make all these parameters learnable, which makes GLIF neurons adjust their neuronal dynamics during training, increasing the adaptivity of the spiking neurons. Given x is one of these parameters, we can obtain x by:

$$x = \frac{1}{1 + \exp(-x_p)}, \tag{13}$$

where $x_p \in (-\infty, +\infty)$ is shared channel-wisely in SNNs. Consequently, each channel shares a unique setting of GLIF neurons. Thus, the heterogeneity of spiking neurons is significantly increased.

Training framework. In terms of the training framework, we utilize backpropagation through time (BPTT) as the training algorithm for our GLIF SNNs. As for the non-differentiable Heaviside step function in Eq.(6), we solve it by the surrogate gradient defined as:

$$\frac{d\mathbb{H}(x)}{dx} = \text{sign}(x < 0.5). \tag{14}$$

Thus, GLIF SNNs can be trained end-to-end.

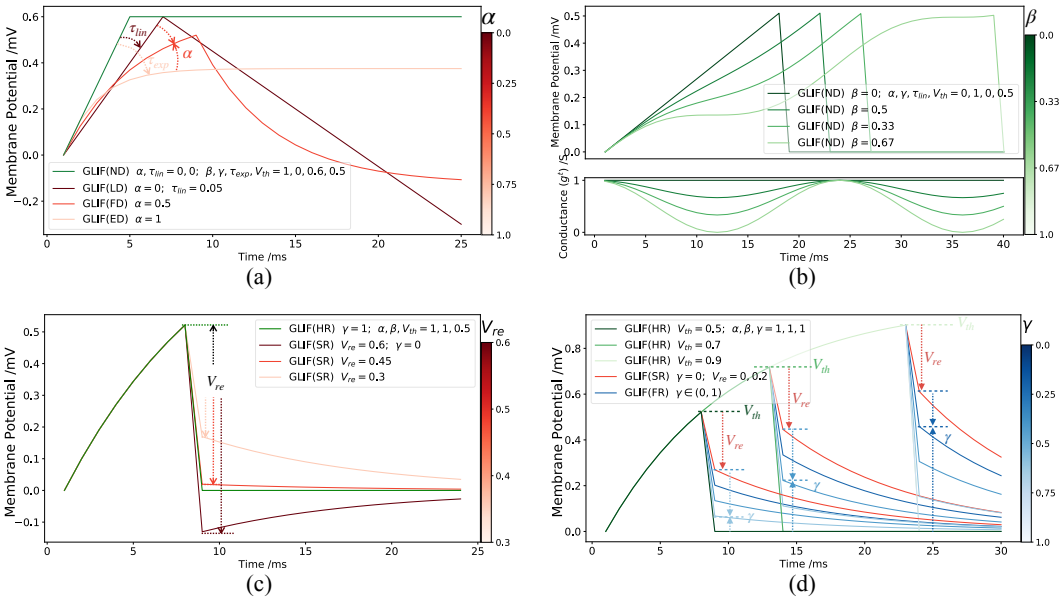

Figure 2: Visualization of neuronal dynamics. (a) The potential trace with α being the variable to bridge the linear and exponential decay. (b) **Upper:** the potential trace with β being the variable to harness the amplitude of the cosine coding pattern. **Lower:** the cosine oscillation of conductance g^t. (c) The potential trace with V_{re} being the variable to display possible scenarios of soft reset in comparison with the hard reset. (d) The potential trace with γ being the variable to bridge the soft and hard reset. Note that **ND** represents non-decay, **LD** linear decay, **ED** exponential decay, **FD** fused decay, **SR** soft reset, **HR** hard reset, and **FR** fused reset.

3.3 Dynamic Analysis

GLIF contains dual bio-features, which brings great diversity to the neuronal dynamics. Here we use a simple case to analyze the dynamic properties of GLIF. Fig. (2) illustrates the response of the spiking neurons to the constant input, which spikes each time step until the membrane potential reaches the threshold. As shown in the figure, GLIF neurons with different parameter configurations have completely different dynamic responses to the same input.

Bridging the gap between exponential decay and linear decay. As shown in Fig. 2(a), compared with non-decay, on the one hand, exponential decay brings the neuronal dynamic with stability and astringency, making it increasingly difficult for the membrane potential to climb over the threshold. However, the membrane potential falls into the saturation zone and fails to reach the potential threshold, which indicates exponential decay may impair the spiking responsiveness. On the other hand, linear decay operates equally at each time step to avoid saturation, thus maintaining the high spiking responsiveness. However, if there are no inputs, linear decay leads to the potential decreasing in an unlimited way, which impairs the stability. While in GLIF, the above two types of decays are the extreme cases, i.e., GLIF only acts exponential decay if $\alpha = 1$ and only serves linear decay if $\alpha = 0$. In most cases where $\alpha \in (0, 1)$, GLIF is eligible for exponential decay's astringency and benefits from the high spiking responsiveness linear decay brings about. To some extent, the gating factor α makes the two decays complementary and determines the proportion of each of the two decays, bridging the gap between the neuronal dynamics of exponential decay and linear decay and enlarging the representation space of membrane potential leakage. Furthermore, since τ_{exp} and τ_{lin} are learnable in GLIF, the gap between exponential and linear decay becomes more flexible. Therefore, the actual representation space given by τ_{exp}, τ_{lin}, and α could be even larger.

Incorporating time-dependent synaptic weights. In GLIF, we assign the time-dependent synaptic weights g^t to the spike train to differentiate spike stimulation levels at different time steps. Since

g^t is learnable, the flexible-coding patterns of different GLIF neurons may differ significantly. For the convenience of analysis, we add constraints to g^t, assuming that g^t is in the form of cosine oscillation, where β controls the amplitude. As shown in Fig. 2(b), when $\beta = 0$, which means the uniform-coding pattern, each time the spiking neuron receives an input spike, the membrane potential increases by the same amount. Our GLIF is different. When $\beta \in (0, 1)$, each time the GLIF receives an input spike, the membrane potential responds differently depending on the specific stimulation level of the current input spike. On the one hand, considering that there is no constraint on g^t in practice, GLIF is more flexible, and the neuronal dynamic diversity is further increased. On the other hand, because the stimulus of input spikes at different times are considered differently, incorporating time-dependent synaptic weights also helps to better process temporal features.

Bridging the gap between hard reset and soft reset. Fig. 2(c) compares the neuronal dynamics between soft reset and hard reset. As we can see, soft reset reduces the current membrane potential by V_{re}. Since V_{re} is not related to the current membrane potential, soft reset may lead to over-resetting or under-resetting of membrane potential, which is flexible for the spiking neurons. Hard reset reduces the current membrane potential to an empirical value, e.g., 0, restarting the potential trace all over, providing the neuronal dynamics with stability. While in GLIF, we consider the potential reduction caused by spike initiation to be both related to V_{re} and the current membrane potential. Because $\gamma \in (0, 1)$ balances the amplitudes of the two resets, GLIF can reset the membrane potential to any possible levels between the consequent potentials of hard reset and soft reset as shown in Fig. 2(d), enlarging the representation space of spike initiation.

4 Experiments

In this section, we demonstrate the effectiveness of our proposed GLIF model. We first compare our results with other existing state-of-the-arts, then carry out ablation studies to evaluate different aspects of our proposed method.

4.1 Experimental Settings

We perform experiments on two kinds of datasets. The first is image classification datasets, including CIFAR[46] and ImageNet[47]. The other one is the event dataset, i.e. DVS128 Gesture[48], which is a gesture recognition dataset captured by DVS cameras. For a fair comparison with other methods, we choose the commonly used network architectures in existing works for experiments, including ResNet-family[49, 9, 44], LIAF-Net[28], 7B-Net[43], and CIFARNet[42, 8, 50], and apply tdBN[9] to all of them. More implementation details of training those SNNs are revealed in Appendix.

4.2 Comparison with Existing Works

CIFAR. We test our GLIF on CIFAR-10 and CIFAR-100 datasets and run three times for each experiment to report the "mean $\pm$ std". As shown in Table 1, our GLIF SNNs can outperform existing works. Specifically, on CIFAR-10, we first test our GLIF on a smaller network CIFARNet and achieve the superior accuracy over other methods [42, 8, 50], even with fewer time steps. Since tdBN is employed in our GLIF SNNs, we then compare GLIF with STBP-tdBN[51] on ResNet-19. By simply changing the neurons in STBP-tdBN to GLIF, our SNNs can achieve significant improvement across all the tested time-steps. Compared with the state-of-the-art TET[12], our method can still obtain better accuracy, and our ResNet-19 with time-step 4 even outperforms theirs with time-step 6 by 0.35%. On CIFAR-100, our method can also achieve much better performance than STBP-tdBN and TET. We also compare GLIF ResNet-18 with the highly handcrafted ResNet-18 of Dspike[11]. As listed in Table 1, our GLIF ResNet-18 can outperform Dspike ResNet-18 by at least 0.63% and 2.92% absolute accuracy on CIFAR-10 and CIFAR-100, respectively.

ImageNet. We apply GLIF to ResNet-34 and MS-ResNet-18[44]. Table 2 shows the results on the validation set. We first compare our method with STBP-tdBN, which can be viewed as our

Table 1: Comparisons with existing works on CIFAR datasets.

Method	Architecture	CIFAR10		CIFAR100	
		TimeStep	Accuracy	TimeStep	Accuracy
STBP[42]	CIFARNet	12	89.83	-	-
STBP NeuNorm[8]	CIFARNet	12	90.53	-	-
TSSL-BP[50]	CIFARNet	5	91.41	-	-
STBP-tdBN[9]	ResNet-19	6	93.16	6	71.12±0.57
		4	92.92	4	70.86±0.22
		2	92.34	2	69.41±0.08
TET[12]	ResNet-19	6	94.50±0.07	6	74.72±0.28
		4	94.44±0.08	4	74.47±0.15
		2	94.16±0.03	2	72.87±0.10
Dspike[11]	ResNet-18*	6	94.25±0.07	6	74.24±0.10
		4	93.66±0.05	4	73.35±0.14
		2	93.13±0.07	2	71.68±0.12
GLIF	CIFARNet	5	93.28	-	-
	ResNet-19	6	**95.03±0.08**	6	**77.35±0.07**
		4	**94.85±0.07**	4	**77.05±0.14**
		2	**94.44±0.10**	2	**75.48±0.08**
	ResNet-18	6	**94.88±0.15**	6	**77.28±0.14**
		4	**94.67±0.05**	4	**76.42±0.06**
		2	**94.15±0.04**	2	**74.60±0.24**

* denotes highly handcrafted network.

Table 2: Comparisons on ImageNet.

Method	Architecture	T	Acc.
TET[12]	ResNet-34	6	64.79
Dspike[11]	ResNet-34	6	68.19
STBP-tdBN[9]	ResNet-34	6	63.72
SEW+PLIF[43]	SEW-ResNet-34	4	67.04
MS-ResNet[44]	MS-ResNet-18	6	63.10
GLIF	ResNet-34	6	**69.09**
	ResNet-34	4	**67.52**
	MS-ResNet-18	6	**68.11**

T denotes the time step.

Table 3: Comparisons on DVS128 Gesture.

Method	Architecture	T	Acc.
DECOLLE[52]	DECOLLE-Net	500	95.54
LIAF+TA[33]	TA-SNN-Net	60	98.61
SEW+PLIF[43]	7B-Net	16	97.92
STBP-tdBN[9]	ResNet-17	40	96.87
LIAF[28]	LIAF-Net	60	97.56
GLIF	7B-Net	16	**100.00±0.00**
	ResNet-17	40	**100.00±0.00**
	LIAF-Net	40	**99.41±0.14**

T denotes the time step.

baseline, on ResNet-34, and we can observe that our GLIF SNNs achieve better performance (69.09% v.s. 63.72%). Since parametric technology is employed in our GLIF, we also compare GLIF with the parametric spiking neuron PLIF[43]. Without changing the model structure, our method can still achieve higher accuracy than PLIF on ResNet-34 (67.52% v.s. 67.04%). Moreover, compared with MS-ResNet[44], whose handcrafted residual block achieves the state-of-the-art performance, we apply our GLIF to MS-ResNet-18 and can also significantly increase the accuracy (68.11% v.s. 63.10%). These results demonstrate the effectiveness of our proposed GLIF model. In addition, compared with other SNNs in TET[12] and Dspike[11], GLIF SNNs can also obtain higher accuracy.

DVS128 Gesture. To show the effectiveness of GLIF in processing spatio-temporal features, we conduct experiments on the event dataset DVS128 Gesture and run each experiment three times to report the "mean $\pm$ std". Since previous works use different network architectures on this dataset, we compare with existing methods PLIF[43], STBP-tdBN[9], and LIAF[28] on 7B-Net, ResNet-17, and LIAF-Net, respectively. As shown in Table 3, our GLIF SNNs can outperform all of those methods, which demonstrates the effectiveness of the proposed GLIF on spatio-temporal event streams.

Table 4: Comparison with different simplex LIFs.

	000	**001**	**010**	**011**	**100**	**101**	**110**	**111**	**GLIF**
ResNet-18	75.77	76.05	74.27	74.59	75.54	75.51	73.36	74.49	**76.39**
ResNet-19	76.29	76.59	73.89	74.71	77.15	76.26	74.39	74.68	**77.22**

Table 5: Ablation study of gating factors.

	GLIF_s	**GLIF_f**	**GLIF**
ResNet-18	76.03	73.56	**76.39**
ResNet-19	76.89	72.78	**77.22**

Table 6: Comparisons with Layer-wise GLIF.

Model	**TimeStep**	**Layer-Wise**	**GLIF**
ResNet-18	4	75.29	**76.34**
	2	73.40	**75.05**
ResNet-19	4	75.71	**77.22**
	2	74.19	**75.54**

4.3 Ablation Study

Effectiveness of different bio-features. To demonstrate the effectiveness of different bio-features that are incorporated in our GLIF, we evaluate the performance of GLIF SNNs in extreme cases where GLIF only acts single bio-feature in each neuronal behavior. Since the gating factors control bio-features, we can obtain eight simplex LIFs by combining different gated biometrics, all of which have static binary gating factors. We name those simplex LIFs with the values of their gating factors, e.g., 101 is the GLIF with $\alpha, \beta, \gamma = 1, 0, 1$ that only acts exponential decay, the uniform-coding pattern, and hard reset. On CIFAR-100, we use ResNet-18 and ResNet-19 with time-step 4 for experiments. As shown in Tabel 4, our proposed GLIF outperforms all of those simplex LIFs, which demonstrates the effectiveness of fusing different bio-features.

Importance of learnable gating factors To demonstrate the effectiveness of our proposed learnable gating factors in fusing bio-features, we compare GLIF with other two GLIF variants: GLIF_s and GLIF_f, where GLIF_s keeps gating factors static after initialization, GLIF_f removes gating-factors and simply fuses two different bio-features by addition. On CIFAR-100, we also use ResNet-18 and ResNet-19 with time-step 4. Table 5 lists the experimental results. On the one hand, compared with GLIF_s, our method can get higher accuracy, which demonstrates that learnable gating factors can make GLIF better. On the other hand, compared with GLIF_f, GLIF can also achieve better performance, this is because learnable gating factors can balance dual bio-features in each neuronal behavior. As as result, learnable gating factors are important in GLIF.

Channel-wise v.s. Layer-wise. Besides the investigations above, we conduct an ablation study on GLIF with different parameter-sharing schemes, which are layer-wise sharing and channel-wise sharing. We use ResNet-19 and ResNet-18 with time-step 2 and 4 on CIFAR-100. As listed in Table 6, GLIF, which leverages channel-wise sharing scheme, consistently improves the performance over the layer-wise sharing method.

5 Conclusion

In this paper, we propose GLIF, a unified spiking neuron, that fuses the bio-features in each neuronal behavior. In GLIF, our method utilizes the gating factor to bridge the gap between the dual bio-features, enhancing the neuronal dynamic diversity and enlarging the representation space of spiking neurons. Furthermore, we adopt the channel-wise parametric method to make all membrane-related parameters learnable, as well as the gating factors, and train those parameters through BPTT, increasing the neuronal adaptivity of spiking neurons. We validate our GLIF SNNs on various benchmark datasets, showing the state-of-the-art performance compared with other methods. Additionally, how to apply GLIF in other training frameworks, e.g., ANN2SNN conversion, remains a worth-studying problem.

References

[1] Wolfgang Maass. Networks of spiking neurons: the third generation of neural network models. *Neural networks*, 10(9):1659–1671, 1997.

[2] Kaushik Roy, Akhilesh Jaiswal, and Priyadarshini Panda. Towards spike-based machine intelligence with neuromorphic computing. *Nature*, 575(7784):607–617, 2019.

[3] Mike Davies, Narayan Srinivasa, Tsung-Han Lin, Gautham Chinya, Yongqiang Cao, Sri Harsha Choday, Georgios Dimou, Prasad Joshi, Nabil Imam, Shweta Jain, et al. Loihi: A neuromorphic manycore processor with on-chip learning. *Ieee Micro*, 38(1):82–99, 2018.

[4] Ziru Li, Bonan Yan, and Hai Li. Resipe: Reram-based single-spiking processing-in-memory engine. In *2020 57th ACM/IEEE Design Automation Conference (DAC)*, pages 1–6. IEEE, 2020.

[5] Weihua He, YuJie Wu, Lei Deng, Guoqi Li, Haoyu Wang, Yang Tian, Wei Ding, Wenhui Wang, and Yuan Xie. Comparing snns and rnns on neuromorphic vision datasets: Similarities and differences. *Neural Networks*, 132:108–120, 2020.

[6] Xiang Cheng, Yunzhe Hao, Jiaming Xu, and Bo Xu. Lisnn: Improving spiking neural networks with lateral interactions for robust object recognition. In *IJCAI*, pages 1519–1525, 2020.

[7] Jing Pei, Lei Deng, Sen Song, Mingguo Zhao, Youhui Zhang, Shuang Wu, Guanrui Wang, Zhe Zou, Zhenzhi Wu, Wei He, et al. Towards artificial general intelligence with hybrid tianjic chip architecture. *Nature*, 572(7767):106–111, 2019.

[8] Yujie Wu, Lei Deng, Guoqi Li, Jun Zhu, Yuan Xie, and Luping Shi. Direct training for spiking neural networks: Faster, larger, better. In *Proceedings of the AAAI Conference on Artificial Intelligence*, volume 33, pages 1311–1318, 2019.

[9] Hanle Zheng, Yujie Wu, Lei Deng, Yifan Hu, and Guoqi Li. Going deeper with directly-trained larger spiking neural networks. In *Proceedings of the AAAI Conference on Artificial Intelligence*, volume 35, pages 11062–11070, 2021.

[10] Wei Fang, Zhaofei Yu, Yanqi Chen, Timothée Masquelier, Tiejun Huang, and Yonghong Tian. Incorporating learnable membrane time constant to enhance learning of spiking neural networks. In *Proceedings of the IEEE/CVF International Conference on Computer Vision*, pages 2661–2671, 2021.

[11] Yuhang Li, Yufei Guo, Shanghang Zhang, Shikuang Deng, Yongqing Hai, and Shi Gu. Differentiable spike: Rethinking gradient-descent for training spiking neural networks. *Advances in Neural Information Processing Systems*, 34, 2021.

[12] Shikuang Deng, Yuhang Li, Shanghang Zhang, and Shi Gu. Temporal efficient training of spiking neural network via gradient re-weighting. In *International Conference on Learning Representations*, 2021.

[13] Andres Upegui, Carlos Andrés Pena-Reyes, and Eduardo Sanchez. An fpga platform for on-line topology exploration of spiking neural networks. *Microprocessors and microsystems*, 29(5):211–223, 2005.

[14] Benjamin Schrauwen, Michiel D'Haene, David Verstraeten, and Jan Van Campenhout. Compact hardware liquid state machines on fpga for real-time speech recognition. *Neural networks*, 21(2-3):511–523, 2008.

[15] Peter U Diehl, Bruno U Pedroni, Andrew Cassidy, Paul Merolla, Emre Neftci, and Guido Zarrella. Truehappiness: Neuromorphic emotion recognition on truenorth. In *2016 international joint conference on neural networks (ijcnn)*, pages 4278–4285. IEEE, 2016.

[16] Peter U Diehl, Guido Zarrella, Andrew Cassidy, Bruno U Pedroni, and Emre Neftci. Conversion of artificial recurrent neural networks to spiking neural networks for low-power neuromorphic hardware. In *2016 IEEE International Conference on Rebooting Computing (ICRC)*, pages 1–8. IEEE, 2016.

[17] Seongsik Park, Seijoon Kim, Byunggook Na, and Sungroh Yoon. T2fsnn: deep spiking neural networks with time-to-first-spike coding. In *2020 57th ACM/IEEE Design Automation Conference (DAC)*, pages 1–6. IEEE, 2020.

[18] Eric R Kandel, James H Schwartz, Thomas M Jessell, Steven Siegelbaum, A James Hudspeth, Sarah Mack, et al. *Principles of neural science*, volume 4. McGraw-hill New York, 2000.

[19] Wulfram Gerstner, Werner M Kistler, Richard Naud, and Liam Paninski. *Neuronal dynamics: From single neurons to networks and models of cognition*. Cambridge University Press, 2014.

[20] Verónica C Piatti, M Georgina Davies-Sala, M Soledad Espósito, Lucas A Mongiat, Mariela F Trinchero, and Alejandro F Schinder. The timing for neuronal maturation in the adult hippocampus is modulated by local network activity. *Journal of Neuroscience*, 31(21):7715–7728, 2011.

[21] Zhisong He and Qianhui Yu. Identification and characterization of functional modules reflecting transcriptome transition during human neuron maturation. *BMC genomics*, 19(1):1–11, 2018.

[22] Frank Bradke, Simone Di Giovanni, and James Fawcett. Neuronal maturation: Challenges and opportunities in a nascent field. *Trends in Neurosciences*, 43(6):360–362, 2020.

[23] Peter Dayan, Laurence F Abbott, et al. Theoretical neuroscience: computational and mathematical modeling of neural systems. *Journal of Cognitive Neuroscience*, 15(1):154–155, 2003.

[24] Andrew Nere, Atif Hashmi, Mikko Lipasti, and Giulio Tononi. Bridging the semantic gap: Emulating biological neuronal behaviors with simple digital neurons. In *2013 IEEE 19th International Symposium on High Performance Computer Architecture (HPCA)*, pages 472–483. IEEE, 2013.

[25] Paul A Merolla, John V Arthur, Rodrigo Alvarez-Icaza, Andrew S Cassidy, Jun Sawada, Filipp Akopyan, Bryan L Jackson, Nabil Imam, Chen Guo, Yutaka Nakamura, et al. A million spiking-neuron integrated circuit with a scalable communication network and interface. *Science*, 345(6197):668–673, 2014.

[26] James E Smith. Efficient digital neurons for large scale cortical architectures. *ACM SIGARCH Computer Architecture News*, 42(3):229–240, 2014.

[27] Filipp Akopyan, Jun Sawada, Andrew Cassidy, Rodrigo Alvarez-Icaza, John Arthur, Paul Merolla, Nabil Imam, Yutaka Nakamura, Pallab Datta, Gi-Joon Nam, et al. Truenorth: Design and tool flow of a 65 mw 1 million neuron programmable neurosynaptic chip. *IEEE transactions on computer-aided design of integrated circuits and systems*, 34(10):1537–1557, 2015.

[28] Zhenzhi Wu, Hehui Zhang, Yihan Lin, Guoqi Li, Meng Wang, and Ye Tang. Liaf-net: Leaky integrate and analog fire network for lightweight and efficient spatiotemporal information processing. *IEEE Transactions on Neural Networks and Learning Systems*, 2021.

[29] Simon Thorpe and Jacques Gautrais. Rank order coding. In *Computational neuroscience*, pages 113–118. Springer, 1998.

[30] Christoph Kayser, Marcelo A Montemurro, Nikos K Logothetis, and Stefano Panzeri. Spike-phase coding boosts and stabilizes information carried by spatial and temporal spike patterns. *Neuron*, 61(4):597–608, 2009.

[31] Jaehyun Kim, Heesu Kim, Subin Huh, Jinho Lee, and Kiyoung Choi. Deep neural networks with weighted spikes. *Neurocomputing*, 311:373–386, 2018.

[32] Seongsik Park, Seijoon Kim, Hyeokjun Choe, and Sungroh Yoon. Fast and efficient information transmission with burst spikes in deep spiking neural networks. In *2019 56th ACM/IEEE Design Automation Conference (DAC)*, pages 1–6. IEEE, 2019.

[33] Man Yao, Huanhuan Gao, Guangshe Zhao, Dingheng Wang, Yihan Lin, Zhaoxu Yang, and Guoqi Li. Temporal-wise attention spiking neural networks for event streams classification. In *Proceedings of the IEEE/CVF International Conference on Computer Vision*, pages 10221–10230, 2021.

[34] Yukun Yang, Wenrui Zhang, and Peng Li. Backpropagated neighborhood aggregation for accurate training of spiking neural networks. In *International Conference on Machine Learning*, pages 11852–11862. PMLR, 2021.

[35] Peter U Diehl, Daniel Neil, Jonathan Binas, Matthew Cook, Shih-Chii Liu, and Michael Pfeiffer. Fast-classifying, high-accuracy spiking deep networks through weight and threshold balancing. In *2015 International joint conference on neural networks (IJCNN)*, pages 1–8. ieee, 2015.

[36] Bodo Rueckauer, Iulia-Alexandra Lungu, Yuhuang Hu, Michael Pfeiffer, and Shih-Chii Liu. Conversion of continuous-valued deep networks to efficient event-driven networks for image classification. *Frontiers in neuroscience*, 11:682, 2017.

[37] Romain Zimmer, Thomas Pellegrini, Srisht Fateh Singh, and Timothée Masquelier. Technical report: supervised training of convolutional spiking neural networks with pytorch. *arXiv preprint arXiv:1911.10124*, 2019.

[38] Nitin Rathi and Kaushik Roy. Diet-snn: Direct input encoding with leakage and threshold optimization in deep spiking neural networks. *arXiv preprint arXiv:2008.03658*, 2020.

[39] Christoph Stöckl and Wolfgang Maass. Optimized spiking neurons can classify images with high accuracy through temporal coding with two spikes. *Nature Machine Intelligence*, 3(3):230–238, 2021.

[40] David E Rumelhart, Geoffrey E Hinton, and Ronald J Williams. Learning representations by back-propagating errors. *nature*, 323(6088):533–536, 1986.

[41] Sander M Bohte, Joost N Kok, and Johannes A La Poutré. Spikeprop: backpropagation for networks of spiking neurons. In *ESANN*, volume 48, pages 419–424. Bruges, 2000.

[42] Yujie Wu, Lei Deng, Guoqi Li, Jun Zhu, and Luping Shi. Spatio-temporal backpropagation for training high-performance spiking neural networks. *Frontiers in neuroscience*, 12:331, 2018.

[43] Wei Fang, Zhaofei Yu, Yanqi Chen, Tiejun Huang, Timothée Masquelier, and Yonghong Tian. Deep residual learning in spiking neural networks. *Advances in Neural Information Processing Systems*, 34, 2021.

[44] Yifan Hu, Yujie Wu, Lei Deng, and Guoqi Li. Advancing residual learning towards powerful deep spiking neural networks. *arXiv preprint arXiv:2112.08954*, 2021.

[45] Wenzhe Guo, Mohammed E Fouda, Ahmed M Eltawil, and Khaled Nabil Salama. Neural coding in spiking neural networks: A comparative study for robust neuromorphic systems. *Frontiers in Neuroscience*, 15:212, 2021.

[46] Alex Krizhevsky, Geoffrey Hinton, et al. Learning multiple layers of features from tiny images. 2009.

[47] Jia Deng, Wei Dong, Richard Socher, Li-Jia Li, Kai Li, and Li Fei-Fei. Imagenet: A large-scale hierarchical image database. In *2009 IEEE conference on computer vision and pattern recognition*, pages 248–255. Ieee, 2009.

[48] Arnon Amir, Brian Taba, David Berg, Timothy Melano, Jeffrey McKinstry, Carmelo Di Nolfo, Tapan Nayak, Alexander Andreopoulos, Guillaume Garreau, Marcela Mendoza, et al. A low power, fully event-based gesture recognition system. In *Proceedings of the IEEE conference on computer vision and pattern recognition*, pages 7243–7252, 2017.

[49] Kaiming He, Xiangyu Zhang, Shaoqing Ren, and Jian Sun. Deep residual learning for image recognition. In *Proceedings of the IEEE conference on computer vision and pattern recognition*, pages 770–778, 2016.

[50] Wenrui Zhang and Peng Li. Temporal spike sequence learning via backpropagation for deep spiking neural networks. *Advances in Neural Information Processing Systems*, 33:12022–12033, 2020.

[51] Abhronil Sengupta, Yuting Ye, Robert Wang, Chiao Liu, and Kaushik Roy. Going deeper in spiking neural networks: Vgg and residual architectures. *Frontiers in neuroscience*, 13:95, 2019.

[52] Jacques Kaiser, Hesham Mostafa, and Emre Neftci. Synaptic plasticity dynamics for deep continuous local learning (decolle). *Frontiers in Neuroscience*, 14:424, 2020.